

A comparative interplay between small heterorings and hypofluorous acids

Boaz G. Oliveira¹

Received: 13 July 2015 / Accepted: 25 September 2015 / Published online: 16 October 2015
© Springer-Verlag Berlin Heidelberg 2015

Abstract Through the B3LYP/6-311++G(d,p) calculations, theoretical studies of structural parameters, electronic properties, infrared vibration modes, and charge density topologies on the $C_2H_4O \cdot HX$ and $C_2H_5N \cdot HX$ ($X = F$ or $O-F$) heterocyclic hydrogen complexes are presented. The H-bond distances and high energies point out strong contacts and stable interactions in these complexes, and the relationships between the frequency shifts on the H-F and H-O bonds as well as O-F σ -holes with the interaction strength are the benchmarks of this current work. The computations of charge transfer amounts in light of the ChelpG and NBO approaches revealed a separation of charge density on the O-F σ -holes, whose statement is reinforced by the QTAIM descriptors. Despite that O-H and N-H H-bonds have been characterized as closed-shell interactions, qualitatively the appearance of a partial covalent profile also was unveiled by the QTAIM protocol.

Keywords Covalent · Heterocyclic · Hydrogen bonds · NBO · QTAIM

Introduction

In recent years, the research works in intermolecular chemistry attained an excellence state with high complexity levels

Electronic supplementary material The online version of this article (doi:10.1007/s00894-015-2829-4) contains supplementary material, which is available to authorized users.

✉ Boaz G. Oliveira
boazgaldino@gmail.com

¹ Instituto de Ciências Ambientais e Desenvolvimento Sustentável, Universidade Federal da Bahia, 47801-100 Barreiras, Brazil

[1–4]. In spite of the experimental procedures or theoretical methods widely used in the studies of intermolecular chemistry [5–7], the benchmark of a weakly bound system is the knowledge of its properties [8, 9], in particular those derived from spectroscopy analyses [10]. As such, one of the most important properties is the stretch frequency shifted to downward values or upward ones [11–14], which are known as red and blue shifts [15, 16]. In the preamble of the intermolecular chemistry, these vibration modes are constantly manifesting on the proton donors, and ideally, the increase and decrease of their bond lengths are testified [17–19]. Meanwhile, the association between the frequency shifts and the intermolecular strength points out that the stretch frequency of the proton donor is shifted to red or blue if the system is weak or strongly bound [20], respectively. Actually, these relationships are valid only if the hybridization on the orbitals of the proton donor bonds outweighs the hyperconjugation phenomenology based on the charge transfer [21].

Nevertheless, among the large set of intermolecular systems stabilized via hydrogen bonds, halogen bonds, dihydrogen bonds or hydride bonds [22–24], in all of them the stretch frequencies of their proton donors shift to red or blue independently of the interaction strength [25]. In line with this in parts, some time ago some theoretical studies of hydrogen-bonded complexes formed by heterocycles and monoprotic acids revealed the appearance of frequencies shifted to the red in the hydrofluoric acid as well as in the hydrochloric acid [26–28]. Unlike the downward vibration mode, the great goal of all these reports was based on the unveiling of the noncovalent character with interaction energies in the range of 50 kJ mol^{-1} . In addition to that, other proton donors with blue shift characteristics interact weakly with heterocycles, e.g., F_3CH and C_2H_4O upon the formation of the $C_2H_4O \cdot HCF_3$ complex with two hydrogen bonds, namely O-H (primary on the lone electron pairs of oxygen)

and F–H (secondary on the axial hydrogen atoms of the ring [27, 29]. In another situation, the properties of a particular class of proton donors with dual interaction features have been documented [30]. Widely known as hypofluorous acid, this proton donor symbolized by HOX (X represents halogen elements, in this case fluorine) is suitable to form pnictogen bonds, hydrogen bonds, halogen bonds or dihydrogen bonds [31–36]. In this current work, a theoretical study about the formation of the $C_2H_4O \cdots HOF$ and $C_2H_5N \cdots HOF$ complexes will be carried out in order to unveil the frequency shifts in the H–O bonds, and in addition to that, a comparison with the $C_2H_4O \cdots HF$ and $C_2H_5N \cdots HF$ systems must be worthwhile. Another point of view concerns if these modes manifest toward red or blue fields as well as if both the interaction energies and σ -hole of the O–X bonds [37–39] exert some influence in this regard [40].

Traditionally, the electronic structure methods whose architectures were developed on the basis of the *ab initio* formalism, in particular the post-Hartree-Fock approaches, are known as the most useful and accurate in studies of intermolecular systems [41–43]. On the other hand, even though the density functional calculations have some limitations to account the dispersion forces, the motivation to assume that hybrids are suitable methods to study a large range of systems has never been so evident [44, 45], mainly if the great goal is the formation of hydrogen-bonded systems [46]. Actually, this outcome is delineated by the performances of some functionals, the B3LYP [47–53], for instance. In view of this, the

first aims of this work are the determination of the optimized geometries in deep potential surfaces, whose results must be in consonance with the computations of the interaction energies and infrared spectra of the $C_2H_4O \cdots HX$ and $C_2H_5N \cdots HX$ complexes (X = F or O–F), and then the B3LYP was chosen.

Besides the B3LYP functional, the computational scheme of this work is also embodied by the Bader's quantum theory of atoms in molecules (QTAIM) [54, 55], as well as by the calculations derived from natural bond orbital (NBO) [56]. Regarding the first one, the great aim is the characterization of the O–H and N–H hydrogen bonds through the location of bond critical points (BCP), by which the electronic densities on the chemical bonds can be quantified [57]. In addition, from electronic density can be estimated a series of topological descriptors, namely as Laplacian ($\nabla^2\rho$), kinetic electronic density energy (G), potential electronic density energy (U), and atomic radii (distance from nuclear center to BCP) [58]. Specifically by means of the Laplacian ($\nabla^2\rho$) and -G/U ratio, the interaction strength may be analyzed, and in furtherance, to be correlated with the profiles of the frequency shifts [21, 25]. The NBO calculations point out the contributions of the *s*- and *p*-hybrid orbitals of the HX molecules [40], wherein the frequency shifts can be theoretically unveiled if the manifestation of red shifts and blue shifts are caused by an increase (*p*-hybrid orbitals is enhanced) and decrease (*p*-hybrid orbitals is reduced) of polarization in H–X [59].

Fig. 1 Optimized geometries of the $C_2H_4O \cdots HOF$ (I), $C_2H_4O \cdots HF$ (II), $C_2H_5N \cdots HOF$ (III) and $C_2H_5N \cdots HF$ (IV) heterocyclic hydrogen complexes obtained from B3LYP/6-311++G(d,p) calculations

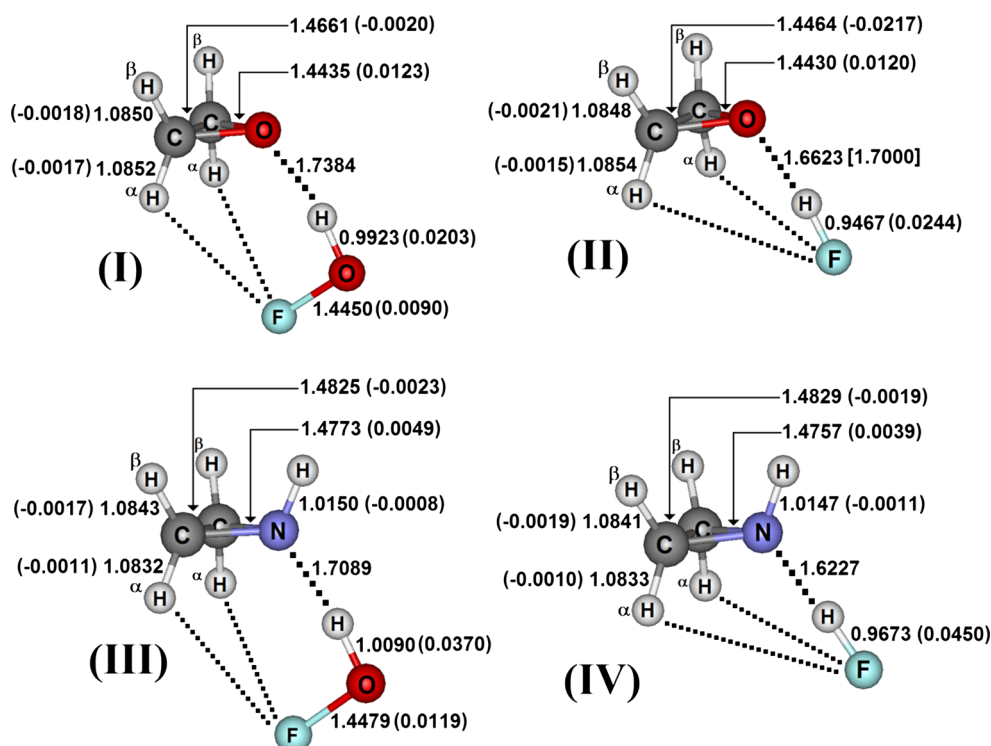


Table 1 Values of the redshifts, absorption intensity ratios, and new vibrational modes of the I-IV heterocyclic hydrogen complexes

IR modes	Isolated proton donors			
	HF	HOF		
$\nu_{\text{H-X}}$	4096.0 (3962.0) ^a	3734.2 (3537) ^b		
$I_{\text{H-X,m}}$	130.1 (77) ^c	47.90		
$\nu_{\text{O-F}}$	—	945.1 (886) ^b		
$I_{\text{O-F,m}}$	—	10.01		
IR modes	Hydrogen complexes			
	I	II	III	IV
$\Delta\nu_{\text{H-X}}$	3362.7 (−371.5)	3557.8 (−538.2)	3020.3 (−713.9)	3135.8 (−960.2)
$I_{\text{H-X,c}}/I_{\text{H-X,m}}$	834.7 (17.4)	1264.8 (9.7)	1475.9 (30.8)	1079.9 (8.3)
$\Delta\nu_{\text{O-F}}$	927.8 (−17.3)	—	921.2 (−23.9)	—
$I_{\text{O-F,c}}/I_{\text{O-F,m}}$	16.4 (1.6)	—	18.4 (1.8)	—
$\nu_{\text{Y-H}}$	242.4	254.3	274.9	281.1
$I_{\text{Y-H}}$	32.2	23.3	26.4	14.9
$\nu_{\text{F-H}}^{\alpha}$	59.24	70.5	54.2	91.0
$I_{\text{F-H}}^{\alpha}$	6.69	6.5	1.9	0.9

Values of ν and I are given in cm^{-1} and km mol^{-1} , respectively

^a Ref. [70]

^b Ref. [71]

^c Ref. [72]

Computational procedure and details

The geometries of the $\text{C}_2\text{H}_4\text{O-HX}$ and $\text{C}_2\text{H}_5\text{N-HX}$ ($\text{X} = \text{F}$ or O-F) complexes were optimized at B3LYP/6-311++G(d,p)

theoretical level with all calculations performed by the GAUSSIAN 03 W and 98 W programs [60]. The optimized geometries of the monomers ($\text{C}_2\text{H}_4\text{O}$, $\text{C}_2\text{H}_5\text{N}$, HOF, and HF) also were obtained through this same theoretical level. The

Table 2 Values of the hydrogen bond energies, variations of dipole moment, ChelpG, and NBO charge transfers (variations in parentheses) of the I-IV heterocyclic hydrogen complexes

Parameters	Hydrogen complexes			
	I	II	III	IV
ΔE	−40.22	−42.99	−56.53	−63.27
ΔZPE	7.12	9.87	7.45	10.76
BSSE	4.57	1.24	5.54	0.64
ΔE^{C}	−28.53	−31.88	−43.54	−51.87
$\Delta\mu$	−0.17	0.46	1.14	1.43
ΔQ^{ChelpG}	−0.056	−0.092	−0.156	−0.225
ΔQ^{NBO}	−0.038	−0.045	−0.065	−0.076
$\Delta q^{\text{H, ChelpG}}$	0.4100 (−0.0040)	0.3940 (−0.0570)	0.3020 (−0.1120)	0.2500 (−0.2010)
$\Delta q^{\text{H, NBO}}$	0.44740 (0.0200)	0.5500 (0.0020)	0.4770 (0.0230)	−0.6200 (−0.0720)
$\Delta q^{\text{O, ChelpG}}$	−0.3530 (−0.6640)	—	−0.3450 (−0.0340)	—
$\Delta q^{\text{O, NBO}}$	−0.325 (−0.0280)	—	−0.3460 (−0.0490)	—
$\Delta q^{\text{F, ChelpG}}$	−0.1130 (−0.0100)	−0.486 (−0.0350)	−0.1130 (−0.0100)	−0.4750 (−0.0240)
$\Delta q^{\text{F, NBO}}$	−0.1870 (−0.0300)	−0.5950 (−0.0470)	−0.1960 (−0.0390)	−0.6200 (−0.0720)

* Values of ΔE , ΔZPE , BSSE, and ΔE^{C} are given in kJ mol^{-1} ;

* Values of $\Delta\mu$ are given in Debye;

* Values of $Q^{\text{H,ChelpG}}$ and $Q^{\text{H,NBO}}$ are 0.414 and 0.454 (HOF), respectively;

* Values of $Q^{\text{O,ChelpG}}$ and $Q^{\text{O,NBO}}$ are −0.311 and −0.297 (HOF), respectively;

* Values of $Q^{\text{F,ChelpG}}$ and $Q^{\text{F,NBO}}$ are −0.103 and −0.157 (HOF), respectively;

* Values of $Q^{\text{H,ChelpG}}$ and $Q^{\text{H,NBO}}$ are 0.451 and 0.548 (HF), respectively;

* Values of $Q^{\text{F,ChelpG}}$ and $Q^{\text{F,NBO}}$ are −0.451 and −0.451 (HF), respectively

hydrogen bond energies have been appraised on the basis of the supermolecule approach, whose values were corrected by the zero-point vibrational energies [61] and values of the basis sets superposition error (BSSE) [62]. The generation of the molecular electrostatic potential (MEP) was performed through the gOpenMol 3.0 graphical program [63, 64]. The QTAIM calculations were processed through the AIMAll 11.19.14 [65] and AIM2000 1.0 [66] topological quantum chemistry packages.

Results and discussion

Structure and infrared spectrum

The optimized geometries of the $C_2H_4O \cdots HOF$ (**I**), $C_2H_4O \cdots HF$ (**II**), $C_2H_5N \cdots HOF$ (**III**), $C_2H_5N \cdots HF$ (**IV**) complexes are illustrated in Fig. 1, in which are also depicted the values of the O–H and N–H H-bond distances as well as the variations in the bond lengths of the H–X proton donor centers (X = F or O–F), the C–N, C–O, and C–C bonds and F–O σ -roles. Regarding the H-bond distances, the complexes **II** and **IV** formed by hydrogen fluoride as proton donor are shorter bound -0.0761 and -0.0862 Å in comparison with the **I** and **III** systems being formed by hypofluorous acid. In spite of the theoretical value of 1.6623 Å [27] being in good agreement with the experimental datum of 1.7000 Å [67], the **IV** complex is the shortest bound one instead of **II**. Furthermore, the complexes of C_2H_5N are shorter bound than those formed by C_2H_4O . In addition, the profile of the H-bond distance must be taken into account to predict drastic structural modifications on these small three-membered rings, one of them is the ring opening. In line with this, it can be perceived that the C–N bond lengths are more markedly enhanced in 0.0049 (**III**) and 0.0039 (**IV**) than 0.0123 (**I**) and 0.0120 Å (**II**) of the C–O bonds. It is important to be stressed that the variation of the C–N and C–O bond lengths is directly proportional to the H-bond distance only regarding the pairs of complexes **I–II** and **III–IV**, and not among them at all.

In comparison with similar heterocyclic systems [27], such as those whose proton donor is HCl, for instance, the H-bond distances of 1.7384 (**I**), 1.6623 (**II**), 1.7089 (**III**), and 1.6227 (**IV**) are slightly longer. Thus, the bond length variations in the proton donors are also less evident, although the values of 0.0370 and 0.0450 Å of **III** and **IV** are more or less twice than 0.0203 and 0.0244 Å of **I** and **II**, respectively. Regarding the O–F σ -hole bonds, the length variation of 0.0090 is incipient in **I**, although the value of 0.0119 Å found for **III** seems in line with the benchmark of proton donors. Some time ago, some works highlighted a certain distortion in the H-bonds, in particular the non-linearity (θ) caused by secondary interactions, which, here, can be interpreted by the F–H $^\alpha$ contact [68]. The θ angle arises when a distortion on the H–X bond is evidenced

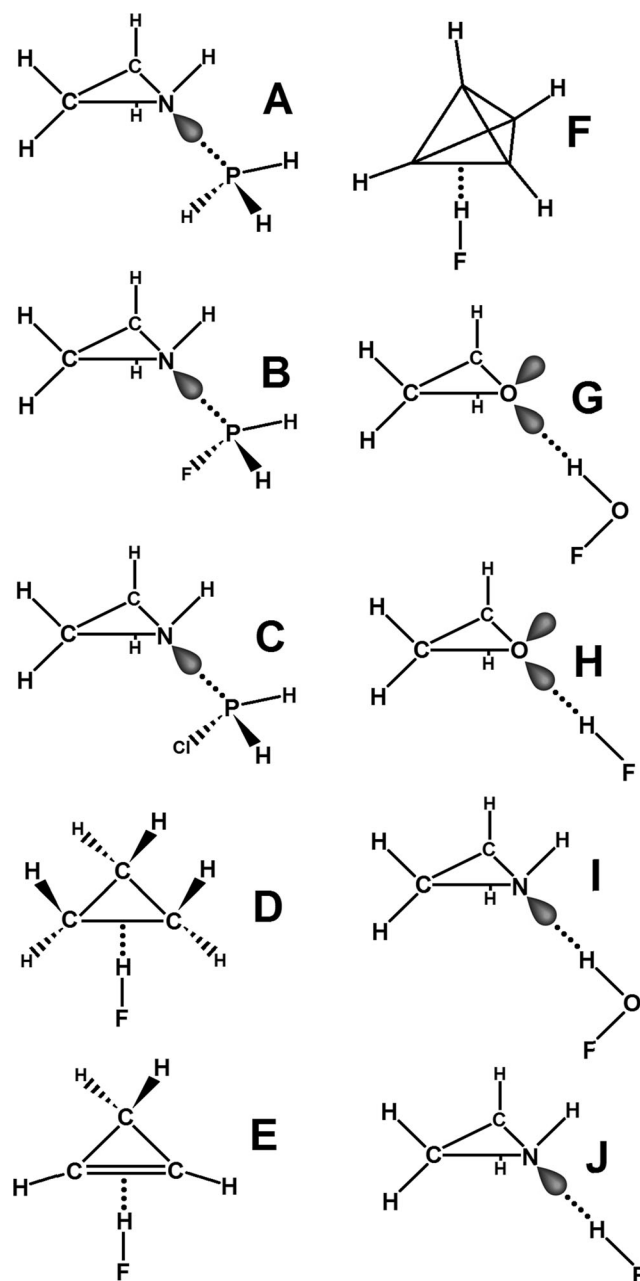


Fig. 2 Heterocyclic hydrogen complexes: Ref. [73]: A, B, and C; Ref. [13]: D, E, and F; Ref. [27]: H and J

due to a misalignment in the YHX axis (Y = O or N and X = F or OF). The computed values for the θ angle at the B3LYP/6-311++G(d,p) level of theory are 10.02 (**I**), 9.2 (**II**), 7.5 (**III**), and 4.1° (**IV**). Even by taking into account that the contact of F–H $^\alpha$ secondary interactions may be feasible, the distance values of 2.9430 (**I**), 3.2732 (**II**), 3.0245 (**III**), and 3.3944 Å (**IV**) are longer than the sum of van der Waals tabulated radii [69] (2.67 Å) which informs that F–H $^\alpha$ is unapproachable. It is not necessary to examine the H-bond distances based on the van der Waals radii because the O–H and N–H contacts are extremely shorter than 2.75 and 2.72 Å. However, a challenge

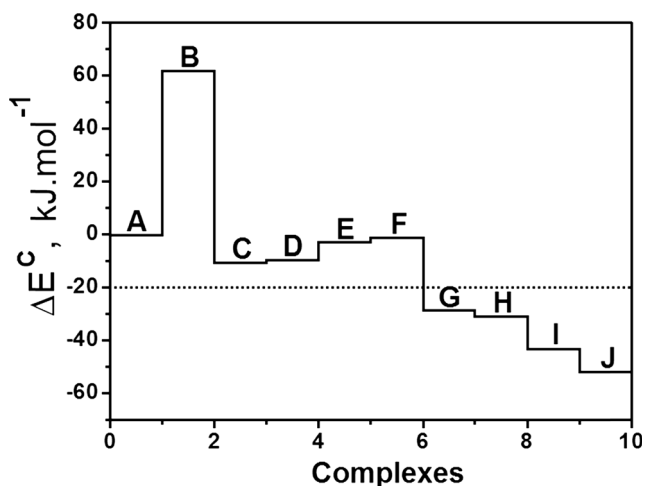


Fig. 3 Comparison among the interaction energies of the complexes pictured in Fig. 2

of distance and strength between the Y–H (Y = O or N) and F–H^α links is stated, wherein once the first type is short (**III** and **IV**) the second one is longer and vice versa (**I** and **II**).

Table 1 lists the values of the infrared vibration modes of HF and HOF monomers and **I**, **II**, **III** and **IV** complexes. Exclusively for the monomers, the theoretical values [27] of the stretch frequencies and absorption intensities are in close agreement with the available experimental data [70–72]. In a parallelism of the stretch frequencies of the H–O bonds before and after complexations of HX with C₂H₄O and C₂H₅N, the computed red shift values are extremely large if compared with other heterocyclic hydrogen-bonded complexes. The absorption intensity ratios values of 17.4 (**I**), 9.7 (**II**), 30.8 (**III**), and 8.3 km mol⁻¹ (**IV**) are not fairly correlated with the respective red shift results of -371.5, -538.2, -713.9 and -960.2 cm⁻¹, in turn these modes are correlated with the intermolecular distance in each pair of complexes. In other

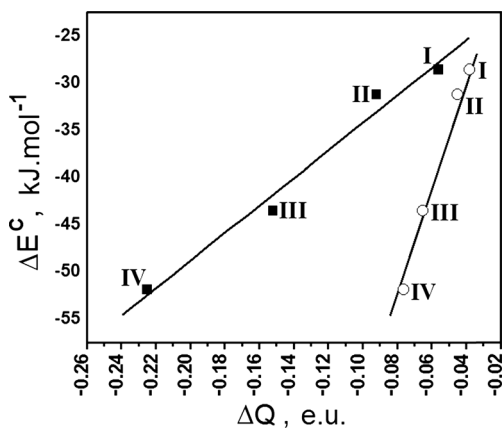


Fig. 4 Relationships between the H-bond energies and transfer transfers

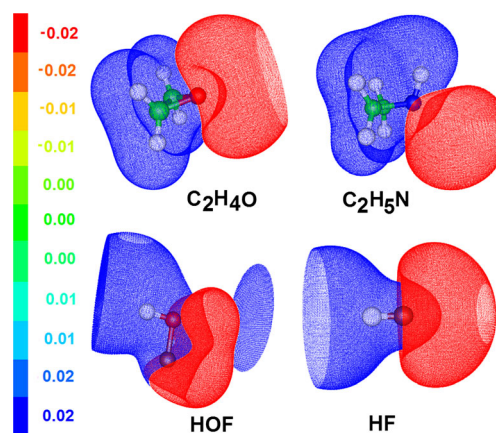


Fig. 5 MEP fields of the C₂H₄O, C₂H₅N, HOF, HOF, and HF monomers. Positive and negative MEP fields are represented by the blue and red isosurfaces, respectively

words, the proton donor frequency shifts are affected by the intermolecular distance, and of course, by the intermolecular strength, actually. As such, the identification of the red shifts on the F–O σ -roles may reinforce the stronger interaction character of the **III** complex in comparison with **I**. This relationship should be testified in this current work, although only later in forward analyses. The identification of the new vibration modes shows that the **III** and **IV** complexes are stronger bound than **I** and **II**. Although the structural analysis has discarded the formation of the secondary interactions between fluorine and axial hydrogen atoms of the C₂H₄O and C₂H₅N 3-membered rings, it was possible to identify the stretch frequencies and absorption intensities of these interactions, whose values of 59.24 (**I**), 70.5 (**II**), 54.2 (**III**), and 91 (**IV**).

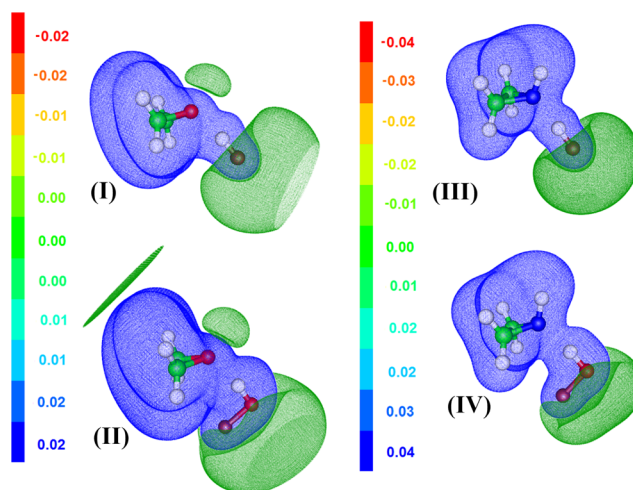


Fig. 6 MEP fields of the C₂H₄O–HOF (**I**), C₂H₄O–HF (**II**), C₂H₅N–HOF (**III**), and C₂H₅N–HF (**IV**) heterocyclic hydrogen complexes. Positive and negative MEP fields are represented by the blue and green isosurfaces, respectively

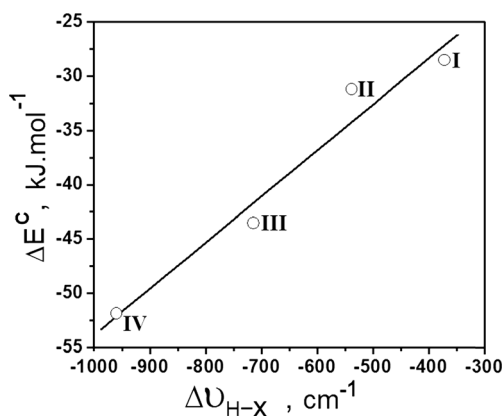


Fig. 7 Relationship between the H-bond energies and frequency shifts

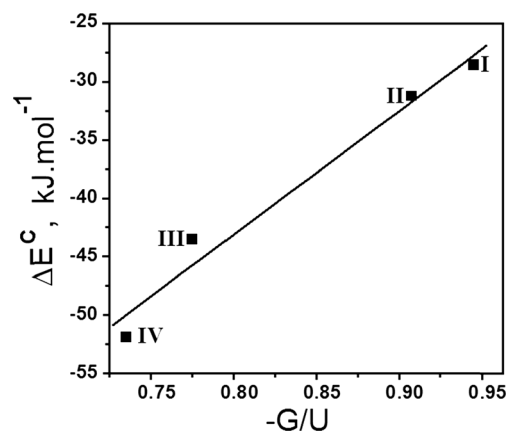


Fig. 8 Relationship between the H-bond energies and kinetic/potential electronic density energy ratios

Interaction energy, dipole moment and charge transfer

The values of the corrected hydrogen bond energies are presented in Table 2. These corrected H-bond energies with variation between -28.53 and -51.87 kJ mol^{-1} represent the peculiar characteristics of the **I-IV** complexes, whose interaction strengths provide a higher stabilization beyond the non-covalent limit [21, 25, 73]. By Fig. 2 and in accordance with Fig. 3, the intermolecular strengths of the heterocyclic complexes are depicted in two facets, namely as: *i*) systems stabilized by n n pnicoxygen bonds whose proton donor is a phosphorus with a lone-electron pair (n) [74] and π H or pseudo- π H hydrogen bonds whose proton acceptor is a π

cloud of hydrocarbons [13]; *ii*) systems stabilized by n H hydrogen bonds whose proton acceptor is a lone-electron pair (n) [27]. Note that, the **III (I)** and **IV (J)** complexes with aziridine are more stabilized than several intermolecular systems. It is through the H-bond energies that a real diagnosis of the interaction strength, and mainly, of the main molecular changes that affect the intermolecular system can be unveiled. As a matter of fact, the values of ΔE^C increase from the **I** complex up to **IV**, and ideally the variations of the dipole moment $\Delta\mu$ also enhances in this same context. Once the dipole moment is closely related with the intermolecular charge transfer in the threshold of HOMO (proton acceptor)

Table 3 Values of the QTAIM topological parameters of the H-F, H-O, and O-F bonds of the **I-IV** heterocyclic hydrogen complexes

BCPs	Hydrogen complexes			
	I	II	III	IV
$\rho_{\text{H-O}}$	0.3392 (-0.0251)	—	0.3198 (-0.0445)	—
$\nabla^2\rho_{\text{H-O}}$	-2.3985 (0.1751)	—	-2.1742 (0.3994)	—
$U_{\text{H-O}}$	-0.7262 (0.0464)	—	-0.6785 (0.0941)	—
$G_{\text{H-O}}$	0.0633 (-0.0013)	—	0.0675 (0.0027)	—
$-G/U_{\text{H-O}}$	0.0871 (0.0034)	—	0.0993 (0.0157)	—
$\rho_{\text{O-F}}$	0.2539 (-0.0085)	—	0.2509 (-0.0115)	—
$\nabla^2\rho_{\text{O-F}}$	0.3197 (0.0220)	—	0.3281 (0.0304)	—
$U_{\text{O-F}}$	-0.3475 (0.0136)	—	-0.3428 (0.0183)	—
$G_{\text{O-F}}$	0.2137 (-0.0040)	—	0.2124 (-0.0052)	—
$-G/U_{\text{O-F}}$	0.6149 (0.0121)	—	0.6196 (0.0168)	—
$\rho_{\text{H-F}}$	—	0.3345 (-0.035)	—	0.3108 (-0.0587)
$\nabla^2\rho_{\text{H-F}}$	—	-2.4326 (0.3674)	—	-2.1149 (0.6851)
$U_{\text{H-F}}$	—	-0.7787 (0.0886)	—	-0.7121 (0.1552)
$G_{\text{H-F}}$	—	0.0853 (0.0017)	—	0.0971 (0.0081)
$-G/U_{\text{H-F}}$	—	0.1095 (0.0131)	—	0.1287 (0.0323)

* Values of ρ and $\nabla^2\rho$ are given in e.a_0^{-3} and e.a_0^{-5} , respectively;

* Values of U and G are given in electronic units

Table 4 Values of the QTAIM topological parameters of the Y H hydrogen bonds of the I-IV heterocyclic hydrogen complexes

BCPs	Hydrogen complexes			
	I	II	III	IV
ρ_{Y-H}	0.0407	0.0467	0.0530	0.0624
$\nabla^2\rho_{Y-H}$	0.1296	0.1495	0.1059	0.1162
U_{Y-H}	-0.0364	-0.0456	-0.0480	-0.0619
G_{Y-H}	0.0344	0.0414	0.0372	0.0455
$-G/U_{Y-H}$	0.9445	0.9078	0.7750	0.7350

* Values of ρ and $\nabla^2\rho$ are given in e.a.₀⁻³ and e.a.₀⁻⁵, respectively;

* Values of U and G are given in electronic units

and LUMO (proton donor) frontier orbitals, the correlation between the ΔE^C values versus charge transfer amounts (ΔQ) must be worthwhile, whose values (Table 2) computed via ChelpG and NBO protocols are illustrated in Fig. 4. As good approaches, two relationships (Eqs. 1 and 2) between ΔE^C and ΔQ with linear coefficients of 0.992 (ChelpG) and 0.996 (NBO) are modeled:

$$\Delta E^C = -19.54 \Delta Q^{\text{ChelpG}} + 145.57, \quad r^2 = 0.992 \quad (1)$$

$$\Delta E^C = -4.13 \Delta Q^{\text{NBO}} + 618.92, \quad r^2 = 0.996. \quad (2)$$

As can be seen, the relationship in light of the NBO data is slightly better correlated than ChelpG. In Table 2 the values of the variation on atomic charges on the hydrogen, oxygen, and fluorine atoms in each one of the I-IV complexes are also organized. In opposition to the ChelpG results of $\Delta q^{\text{H,ChelpG}}$, the description of the intermolecular electronic mechanism by the NBO calculations fails regarding the balance of atomic charges on hydrogen atoms, in which only in IV a gain of electron density is revealed. No matter if by ChelpG or NBO, an increase of charge density is accounted on the

fluorine of both complexes II and IV. However, a drastic increase of charge density on the oxygen rather than the fluorine in the hypofluorous acid seems reasonable to be affirmed due to the ChelpG values of -0.6640 and -0.0100 e.u. in I as well as -0.0340 and -0.0100 e.u. in III. On the other hand, an accentuated equilibrium of charge density along the OF bond is revealed by means of the NBO values of -0.0280 and -0.0300 in I as well as -0.0490 and -0.0390 e.u. in III. Qualitatively, this scenario is consonant with the σ -hole profile once the electronegativities of oxygen and fluorine are fairly similar, and therefore, a separation of charge density leads to a depletion within the internuclear region. Otherwise, this is not observed by means of the analysis of the molecular electrostatic potential, whose picture is illustrated in Fig. 5 (monomers) and Fig. 6 (complexes). Regardless the interaction strength, the complexes formed by C₂H₄O have MEP surfaces varying between -0.02 and 0.02 e.u. whereas the corresponding values for C₂H₅N are -0.04 and 0.04 e.u. Note that the positive MEP fields along the σ -hole are not clear, although the negative MEP regions on oxygen and fluorine (complexes I and III) are well described. The positive MEP site in the O-H and N-H H-bonds show low concentrations of charge density, which may be better examined via QTAIM topography as closed-shell interactions. So, it is not mandatory that electronegative elements display negative MEP sites and vice versa for positive ones, as has been pointed out by Metrangolo et al. [75, 76]. Regardless of the interaction strength, the formation of hydrogen-bonded systems is a process by which some molecular effects should be taken into account. One of them is the frequency shift on the proton donor bond, whose magnitude is directly related with the interaction energy. In line with this, Fig. 7 plots a graph between the corrected H-bond energies and frequency shifts of the H-X bonds (X = F or OF), whose profile yields a linear relationship ruled by Eq. (3) displayed below:

$$\Delta E^C = 0.04 \Delta \nu_{\text{H-X}} - 11.38, \quad r^2 = 0.979. \quad (3)$$

Table 5 Values of the QTAIM topological parameters for the CCY ring (Y = O or N) of the I-IV heterocyclic hydrogen complexes

RCPs	Hydrogen complexes			
	I	II	III	IV
ρ_{CCY}	0.2051 (-0.0039)	0.2050 (-0.0040)	0.2024 (-0.0017)	0.2028 (-0.0013)
$\nabla^2\rho_{\text{CCY}}$	0.3239 (0.0108)	0.3236 (0.0105)	0.2168 (0.0050)	0.2169 (0.0001)
U_{CCY}	-0.3165 (0.0083)	-0.3164 (0.0084)	-0.2927 (0.0032)	-0.2937 (0.0022)
G_{CCY}	0.1987 (-0.0028)	0.1986 (-0.0029)	0.1735 (-0.0009)	0.1740 (-0.0004)

* Values of ρ and $\nabla^2\rho$ are given in e.a.₀⁻³ and e.a.₀⁻⁵, respectively;

* Values of U and G are given in electronic units

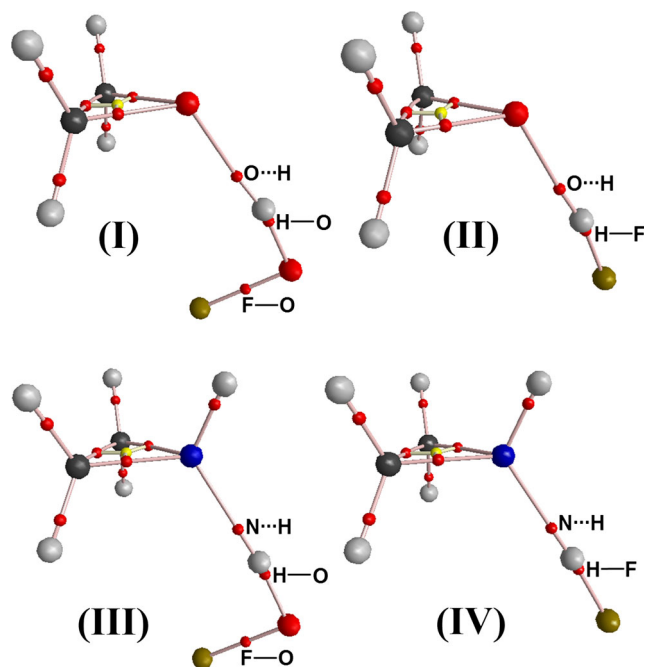


Fig. 9 Bond path, bond critical points, and ring critical points on the $C_2H_4O \cdots HOF$ (**I**), $C_2H_4O \cdots HF$ (**II**), $C_2H_5N \cdots HOF$ (**III**), and $C_2H_5N \cdots HF$ (**IV**) heterocyclic hydrogen complexes

As expected, the largest calculated red shifts of -713.9 and -906.2 cm^{-1} of the **III** and **IV** complexes are in agreement with the high H-bond energies, whereas the **I** and **II** complexes with median interaction strengths, have red shifts that are almost half of the values of **III** and **IV**.

QTAIM parameters and NBO analysis

Table 3 enumerates the results of the QTAIM parameters. The shared interaction profile on the H–F and H–O bond is revealed through the negative Laplacian values and $-G/U_{H-O}$

ratios lower than 0.5. Surely, the shared interaction outcome and covalent character by means of the $-G/U$ ratios with values varying between 0.6149 (**I**) and 0.6196 (**III**) are demonstrated for the O–F bonds. On the other hand, the σ -holes on the O–F bonds are stated in part by the positive Laplacian (0.3197 and 0.3281 e.a_0^{-5}) and smaller electronic density amounts whether compared to those values of H–O. Upon the formation of the **I** and **III** complexes, reductions of electronic density were measured in the range of -0.0251 and $-0.0445 \text{ e.a}_0^{-3}$ (H–O) as well as -0.0085 and $-0.0115 \text{ e.a}_0^{-3}$ (O–F), indicating weakness in the bond strength on the HOF structure. Moreover, increasing the Laplacian values also point out the trend to depletion of charge density in the BCPs of the H–F, H–O, and O–F bonds. Within the intermolecular region, the $Y \cdots H$ H-bonds ($Y = O$ for **I** and **II** whereas $Y = N$ for **III** and **IV**) present low electronic densities ranged from 0.0407 up to 0.0624 e.a_0^{-3} followed by positive Laplacian values of 0.1296 (**I**), 0.1495 (**II**), 0.1059 (**III**), and 0.1162 e.a_0^{-5} (**IV**). However, in accordance with the contributions of the kinetic and potential electronic density energies, the relationship $-G/U$ furnish values smaller than 1.0, specifically 0.9445 (**I**), 0.9078 (**II**), 0.7550 (**III**), and 0.7350 (**IV**), whose profiles corroborate with the high H-bond energies computed previously, indicating that the **I–IV** complexes are partially covalent bound. This insight is useful to predict the interaction strength, and in Fig. 8, a close and excellent relationship ruled by Eq. (4) between the values of ΔE^C and $-G/U_{Y \cdots H}$ give support to the thesis that aziridine supply the heterocyclic strongest hydrogen complexes (Table 4).

$$\Delta E^C = 106.16(-G/U_{Y \cdots H}) - 128 \quad , \quad r^2 = 0.986 \quad (4)$$

Table 5 lists the values of the electronic density, Laplacian, kinetic, and potential electronic density energies for the ring critical points (RCP) within the C_2H_4O and C_2H_5N structures with all values computed after complexation and the variations

Table 6 Values of the QTAIM atomic radii of hydrogen, oxygen, and halogens on the H–O, O–F, and H–F bonds of the **I–IV** heterocyclic hydrogen complexes

Atomic radii	Hydrogen complexes					
	I		II	III		IV
	H–O	O–F	H–F	H–O	O–F	H–F
rH	0.1873 (-0.0068)	—	0.1553 (0.0012)	0.1919 (-0.0022)	—	0.1624 (0.0083)
rO	0.8039 (0.0260)	0.6926 (0.0004)	—	0.8170 (0.0391)	0.6928 (0.0003)	—
rF	—	0.7523 (0.0089)	0.7913 (0.0232)	—	0.7551 (0.0117)	0.8047 (0.0366)

* Values are given in angstroms (\AA);

* H–F: $rH=0.1541 \text{ \AA}$ and $rF=0.7681 \text{ \AA}$;

* H–O: $rH=0.1941 \text{ \AA}$ and $rO=0.7779 \text{ \AA}$;

* O–F: $rO=0.6925 \text{ \AA}$ and $rF=0.7434 \text{ \AA}$

Table 7 Values of the *s*- and *p*-characters of the hybrid orbitals of the H–F, H–O, and O–F bonds of the **I–IV** heterocyclic hydrogen complexes

Hybridizations	Hydrogen complexes					
	I		II	III		IV
	H–O	O–F	H–F	H–O	O–F	H–F
<i>s</i> H	99.77 (–0.040)	—	99.73 (–0.12)	99.77 (–0.040)	—	99.71 (–0.14)
<i>p</i> H	0.23 (0.040)	—	0.27 (0.12)	0.23 (0.040)	—	0.29 (0.14)
<i>s</i> O	25.19 (4.400)	6.65 (–0.830)	—	27.57 (6.78)	6.50 (–0.98)	—
<i>p</i> O	74.70 (–4.380)	93.20 (0.880)	—	72.33 (–6.75)	93.36 (1.04)	—
<i>s</i> F	—	8.47 (0.060)	24.93 (4.63)	—	8.59 (0.18)	27.33 (7.03)
<i>p</i> F	—	91.41 (–0.070)	74.98 (–4.61)	—	91.30 (–0.18)	72.59 (–7.00)

All values are given in %;

* H–F: *s*H=99.85 %, *p*H=0.15 %, *s*F=20.30 % and *p*F=79.59 %;

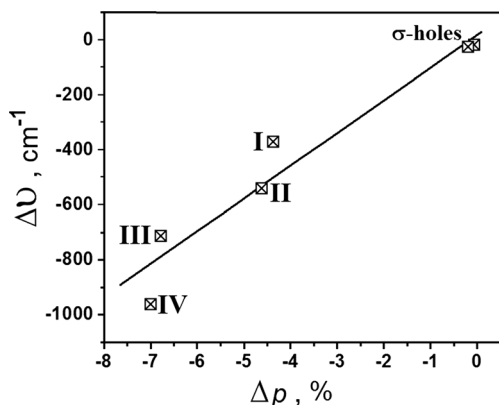
* H–O: *s*H=99.81 %, *p*H=0.19 %, *s*O=20.79 % and *p*O=79.08 %;

* O–F: *s*O=7.48 %, *p*O=92.32 %, *s*F=8.41 % and *p*F=91.48 %

in parentheses. Another indication of the strain ring relaxation are the reductions of –0.0038 (**I**), –0.0040 (**II**), –0.0017 (**III**), and –0.0013 (**IV**) of the electronic densities. Of course these electronic density amounts are smaller than those determined at each BCP because the electron flux on RCP is sensitively reduced, but it can be seen that no relationship between these variations and interaction strength seem to be valued. Throughout this work, a clear mention regarding the formation of secondary interactions have been discussed either by structural or vibrational data. The locations of BCPs between F and H^α would lead to the formation of double RCPs with five (**II** and **IV**) and six (**I** and **III**) members. Due to this, the F–H^α contact would be validated, contributing decisively for the

stabilization of the **I–IV** complexes. As can be seen in Fig. 9, besides the RCPs (C–C–Y with Y = O or N), the BCPs along the C–H, C–C, C–Y, Y–H, H–F, H–O, and O–F, any BCPs between F and H^α were not localized by the QTAIM calculations in order to characterize the secondary interaction F–H^α.

In QTAIM, the BCP is a descriptor located in a bond path which interconnects two nuclei. Dealing with this, the single distance between each nucleus is considered a QTAIM atomic radius, which can vary whenever the position of the BCP move along the bond path. Table 6 lists the values of the QTAIM radii of the hydrogen, oxygen, and fluorine of both HF and HOF followed by the variations upon the formation of the **I–IV** complexes. On the fluoride of the hydrofluoric acid are observed the greater variations of atomic radii, whose values of Δr_F are 0.0232 (**II**) and 0.0366 Å (**IV**). Otherwise, the most incisive variations on hypofluorous acid are related to the oxygen in the H–O bond, whose values of 0.0260 (**II**) and 0.0391 Å (**III**) are slightly greater than 0.0232 (**II**) and 0.0366 Å (**IV**) of the fluoride in the O–F bonds. In line with this, Table 7 gathers the values of the *s*- and *p*-hybrid orbitals computed it light of the NBO approach for the H–F, H–O, and O–F bonds of the **I–IV** complexes. Firstly, in the HF bonds is observed a percentage increase of the *s*F orbital whereas the *p*F is reduced. It would be expected a direct relationship between the *p*F reductions of –4.61 (**II**) and –7.00 % (**IV**) with reduction of the fluoride radius, although, undoubtedly this does not occur because the *r*F enlarges. In fact, once these *s*- and *p*-contributions are connected with the hybrid orbital, and in the sense of weakening of the H–F bond detected by the red

**Fig. 10** Relationship between the frequency shifts and variations on the *p*-hybrid orbitals

shifts, certainly the contribution of the pF orbital must be reduced in this regard. In HOF molecule, however, the most drastic variations of hybrid orbitals concerns the H–O bonds, ideally because the red shifts on this oscillator are much more evident rather than those computed to the O–F bond. The values of sO and pO in **I** are 4.400 and -4.380% whereas in **II** are 6.78 and -6.75% , respectively. Note that the contributions of the p -hybrid orbitals are always diminishing. To the best of our knowledge, a relationship is established between the frequency shifts and variations of the p -hybrid orbitals (Eq. 5), such as is illustrated in Fig. 10.

$$\Delta\nu = 118.93\Delta\nu_{H-X} + 18.79, \quad r^2 = 0.967 \quad (5)$$

The benchmark of the s - and p -contributions regarding the electropositive and electronegative elements (hydrogen and fluoride or oxygen) must display the Bent's rule of the chemical bond [77]. Once the red shifts have been characterized in the HF and HO bonds, an increase of polarization in light of p -orbitals moieties was expected. However this scenery was not possible because these orbitals represent a hybrid one, and if the weakening of the proton donor bond is quoted, surely its p -contribution must be decreased.

Conclusions

The formation of H-bonds in the C_2H_4O HOF, C_2H_4O HF, C_2H_5N HOF, and C_2H_5N HF heterocyclic complexes was discussed here from the theoretical viewpoint. The good agreement between the bond length enhancements and frequency shifts was established, although the red shift values of the H–F and H–O bonds are much more evident than those of the O–F σ -holes. In fact, the close relationship between the corrected H-bond energies and frequency shifts of the H–F and H–O bonds show the influence of the interaction strength in this regard. In addition, the charge transfer amounts also reveal linear and systematic tendencies with the red shift values. Besides the short H-bond distances followed by the intense new vibration modes and high H-bond energies ($< -50 \text{ kJ}\cdot\text{mol}^{-1}$), the QTAIM calculations pointed out a partial covalence feature in the O–H and N–H bonds. Once again regarding the interaction strength, which shows itself partially covalent in the C_2H_4O HOF, C_2H_4O HF, C_2H_5N HOF, and C_2H_5N HF complexes, the frequency shifts values agree well with the H-bond energies. At last, was modeled another linear and efficient relationship between the red shifts and the variation on the p -orbital of the HX bonds, including until the σ -holes.

Acknowledgments FAPESB, CAPES, and CNPq Brazilian Funding Agencies

References

- Lehn J-M (2002) Proc Natl Acad Sci U S A 99:4763–4768
- Ramasesha K, De Marco L, Mandal A, Tokmakoff A (2013) Nat Chem 5:935–940
- Israelachvili J, Ruths M (2013) Langmuir 29:9605–9619
- Clark GR, Pytel PD, Squire CJ (2012) Nucleic Acids Res 40:5731–5738
- Dykstra CE, Lisy JM (2000) J Mol Struct (THEOCHEM) 500:375–390
- Ding S, Song L-J, Chung LW, Zhang X, Sun J, Wu Y-D (2013) J Am Chem Soc 135:13835–13842
- Fager-Jokela E, Muuronen M, Khaizourane H, Vázquez-Romero A, Verdaguer X, Riera A, Helaja J (2014) J Org Chem 79:10999–11010
- Knowles TP, Fitzpatrick AW, Meehan S, Mott HR, Vendruscolo M, Dobson CM, Welland ME (2007) Science 318:1900–1903
- Graham KR, Cabanetos C, Jahnke JP, Idso MN, El Labban A, Ndjawa GON, Heumueller T, Vandewal K, Salleo A, Chmelka BF, Amassian A, Beaujuge PM, McGehee MD (2014) J Am Chem Soc 136:9608–9618
- Andersen J, Heimdal J, Mahler DW, Nelander B, Larsen RW (2014) J Chem Phys 140:091103–091105
- Oliveira BG, Leite LFCC (2009) J Mol Struct (THEOCHEM) 915:38–42
- Oliveira BG, Araújo RCMU, Ramos MN (2010) J Mol Struct (THEOCHEM) 944:168–172
- Oliveira BG, Araújo RCMU, Ramos MN (2009) J Mol Struct (THEOCHEM) 908:79–83
- Oliveira BG, Lima MCA, Pitta IR, Galdino SL, Hernandes MZ (2010) J Mol Model 16:119–127
- Jabłoński M (2014) J Comput Chem 35:1739–1747
- Karpfen A (2011) Phys Chem Chem Phys 13:14194–14201
- Li AY (2007) J Chem Phys 126:154102–154111
- Oliveira BG, Araújo RCMU, Ramos MN (2009) Orbital Electron J Chem 1:156–166
- Oliveira BG, Araújo RCMU, Carvalho AB, Ramos MN (2009) Orbital Electron J Chem 1:167–182
- Grabowski SJ (2011) J Phys Chem A 115:12789–12799
- Grabowski SJ (2011) Chem Rev 111:2597–2625
- Oliveira BG, Ramos MN (2010) Int J Quantum Chem 110:307–316
- Oliveira BG (2012) Comput Theor Chem 998:173–182
- Oliveira BG, Araújo RCMU, Leite ES, Ramos MN (2011) Int J Quantum Chem 111:111–116
- Oliveira BG (2013) Phys Chem Chem Phys 15:37–79
- Oliveira BG, Araújo RCMU, Carvalho AB, Ramos MN (2007) Spectrochim Acta A 68:626–631
- Oliveira BG, Araújo RCMU, Carvalho AB, Ramos MN (2009) J Mol Model 15:421–432
- Oliveira BG, Araújo RCMU, Carvalho AB, Ramos MN (2011) J Mol Model 17:2847–2862
- Hobza P, Havlas Z (2000) Chem Rev 100:4253–4264
- Li Q-Z, Jing B, Li R, Liu Z-B, Li W-Z, Luan F, Cheng J-B, Gong B-A, Sun J-Z (2011) Phys Chem Chem Phys 13:2266–2271
- An X, Zhuo H, Wang Y, Li Q (2013) J Mol Model 19:4529–4535
- Del Bene JE, Alkorta I, Elguero J (2015) Noncovalent forces: challenges and advances in computational chemistry and physics 19:191–263
- Li Q, Zhu H, Zhuo H, Yang X, Li W, Cheng J (2014) Spectrochim Acta A 132:271–277
- Oliveira BG, Vasconcellos MLLA (2009) Inorg Chem 12:1142–1144
- Oliveira BG, Vasconcellos MLLA (2009) Struct Chem 20:897–902
- Oliveira BG, Araújo RCMU, Silva JJ, Ramos MN (2010) Struct Chem 21:221–228

37. Murray JS, Lane P, Politzer P (2009) *J Mol Model* 15:723–729
38. Politzer P, Murray JS, Clark T (2013) *Phys Chem Chem Phys* 15: 11178–11189
39. Donald KJ, Tawfik M (2013) *J Phys Chem A* 117:14176–14183
40. Oliveira BG, Zabardasti A, Goudarziafshar H, Salehnassaj M (2015) *J Mol Model*. doi:10.1007/s00894-015-2616-2
41. Rezáč J, Riley KE, Hobza P (2012) *J Comput Chem* 33:691–694
42. Mendizabal F, Miranda-Rojas S, Barrientos-Poblete L (2015) *Comput Theor Chem* 1057:74–79
43. Oliveira BG, Araújo RCMU, Carvalho AB, Ramos MN, Hernandez MZ, Cavalcante KR (2007) *J Mol Struct (THEOCHEM)* 802:91–97
44. Molina R, Stella S, Redondo P, Gomez H, Marcaida MJ, Orozco M, Prieto J, Montoya G (2015) *Nat Struct Mol Biol* 22:65–75
45. Ramakrishnan R, Dral PO, Rupp M, von Lilienfeld A *Scien Data* doi:10.1038/sdata.2014.22
46. Briggs EA, Besley NA (2014) *Phys Chem Chem Phys* 16:14455–14462
47. Sánchez-de-Armas R, Ahlquist MSG (2012) *Phys Chem Chem Phys* 17:812–816
48. Walker M, Harvey AJA, Sen A, Dessent CEH (2013) *J Phys Chem A* 117:12590–12600
49. Martínez-Cifuentes M, Weiss-López BE, Santos LS, Araya-Maturana R (2014) *Molecules* 19:9354–9368
50. Fedorova IV, Kiselev MG, Safonova LP (2015) *J Mol Model* 21: 17–22
51. Szafran M, Komasa A, Ostrowska K, Katrusiak A, Dega-Szafran Z (2015) *Spectrochim Acta A* 136:1216–1226
52. Li L, Wu C, Wang Z, Zhao L, Li Z, Sun C, Sun T (2015) *Spectrochim Acta A* 136:338–346
53. Kollenz G, Smounig R, Belaj F, Kvaskoff D, Wentrup C (2015) *Beilstein J Org Chem* 11:1–8
54. Bader RFW (1990) *Atoms in molecules - A quantum theory*. Oxford University Press, Oxford
55. Bader RFW (1991) *Chem Rev* 91:893–928
56. Glendening ED, Landis CR, Weinhold F (2012) *WIREs Comput Mol Sci* 2:1–4
57. Oliveira BG (2014) *Struct Chem* 25:745–753
58. Oliveira BG (2014) *Spectrochim Acta A* 124:208–215
59. Santos ITO, Rego DG, Oliveira BG (2014) *Quim Nov.* 37:624–630
60. Frisch MJ, Trucks GW, Schlegel HB, Scuseria GE, Robb MA, Cheeseman JR, Montgomery JA, Vreven T, Kudin KN, Burant JC, Millam JM, Iyengar SS, Tomasi J, Barone V, Mennucci B, Cossi M, Scalmani G, Rega N, Petersson GA, Nakatsuji H, Hada M, Ehara M, Toyota K, Fukuda R, Hasegawa J, Ishida M, Nakajima T, Honda Y, Kitao O, Nakai H, Klene M, Knox JE, Hratchian HP, Cross JB, Adamo C, Jaramillo J, Gomperts R, Stratmann RE, Yazyev O, Austin AJ, Cammi R, Pomelli C, Ochterski JW, Ayala PY, Morokuma K, Voth GA, Salvador P, Dannenberg JJ, Zakrzewski VG, Dapprich S, Daniels AD, Strain MC, Farkas O, Malick DK, Rabuck AD, Raghavachari K, Foresman JB, Ortiz JV, Cui Q, Baboul AG, Clifford S, Cioslowski J, Stefanov BB, Liu G, Liashenko A, Piskorz P, Komaromi I, Martin RL, Fox DJ, Keith T, Al-Laham MA, Peng CY, Nanayakkara A, Challacombe M, Gill PMW, Johnson B, Chen W, Wong MW, Gonzalez C, Pople JA (2003) *Gaussian 03*. Gaussian Inc, Pittsburgh
61. Rahal M, Hilali M, El Hammadi A, El Mouhtadi M, El Hajbi A (2001) *J Mol Struct (THEOCHEM)* 572:73–80
62. Boys SF, Bernardi F (1970) *Mol Phys* 19:553–566
63. Laaksonen L (1992) *J Mol Graph* 10:33–34
64. Bergman DL, Laaksonen L, Laaksonen A (1997) *J Mol Graph Model* 15:301–306
65. Keith TA (2011) *AIMAll (Version 11.10.16)*, TK Gristmill Software, Overland Park
66. Biegler-König F, Bayles D, Schönbohm J (2000) *AIM2000 1.0*, University of Applied Sciences, Bielefeld
67. Legon AC, Kisiel Z, Georgiou AS, Millen DJ (1989) *Chem Phys Lett* 155:447–454
68. Oliveira BG, Araújo RCMU, Carvalho AB, Ramos MN (2007) *Quim Nov.* 30:1167–1170
69. Huheey JE, Keiter EA, Keiter RL (1997) *Inorganic chemistry: principles of structure and reactivity*, 4th edn. Prentice Hall, New York
70. Johnson GL, Andrews L (1980) *J Am Chem Soc* 102:5736–5741
71. Shimanouchi T (1977) *J Phys Chem Ref Data* 6:993–1102
72. Bishop DM, Cheung LM (1982) *J Phys Chem Ref Data* 11:119–133
73. Oliveira BG (2014) *Chem Phys* 443:67–75
74. Oliveira BG, Araújo RCMU (2012) *J Mol Model* 18:2845–2854
75. Metrangolo P, Murray JS, Pilati T, Politzer P, Resnati G, Terraneo G (2011) *Cryst Growth Des* 11:4238–4246
76. Metrangolo P, Murray JS, Pilati T, Politzer P, Resnati G, Terraneo G (2011) *CrystEngComm* 13:6593–6596
77. Bent HA (1961) *Chem Rev* 61:275–311